JOURNAL OF AIRCRAFT
Vol. 37, No. 3, May–June 2000

# Validation of a Rotorcraft Mathematical Model for Autogyro Simulation

S. S. Houston*
*University of Glasgow, Glasgow, Scotland G12 8QQ, United Kingdom*

**Results are presented from a study undertaken to validate a rotorcraft mathematical model for simulation of autogyro flight. Although this class of rotary-wing aircraft has found limited application in areas other than sport or recreational flying, commercial interest is increasing. A sparse contemporary literature on autogyro flight emphasizes the timeliness of this work, which takes advantage of flight experiments using a fully instrumented autogyro. Validation is based on comparisons of trim, linearized six-degree-of-freedom derivatives, and time history response of the full nonlinear model to control inputs. The validation process is a vital ingredient in defining the applicability of a mathematical model as an engineering tool for supporting studies into aircraft stability, control, and handling qualities. The model is of generic, nonlinear, individual blade/blade element type, and its configuration as an autogyro is described. It is concluded that simulation of autogyro flight presents no particular difficulties for a generic rotorcraft model. Limitations in predictive capability are clearly delineated, although in general comparisons between flight and theory are good.**

## Nomenclature

| | |
|---|---|
| $A$ | = matrix of state vector acceleration coefficients; linearized model system matrix |
| $A_{11}$, etc. | = minors of linearized system matrix $A$ |
| $a_x^{\text{hinge}}$, $a_z^{\text{hinge}}$ | = hinge acceleration components, m/s$^2$ |
| $B_1$, $B_2$ | = minors of linearized control matrix |
| $C_0$ | = apparent mass factor |
| $I_{\text{flap}}$, $I_{\text{pitch}}$, $I_{\text{lag}}$ | = blade moments of inertia, Nm$^2$ |
| $\boldsymbol{L}$ | = rotor moment vector, Nm |
| $[L]$ | = dynamic inflow static gain matrix |
| $L_{\text{aero}}$ | = aerodynamic rolling moment, Nm |
| $L_v$, $L_p$, etc. | = rolling moment derivatives, 1/(ms), 1/s, etc. |
| $M_{\text{aero}}$ | = aerodynamic pitching moment, Nm |
| $M_{\text{flap}}^{\text{bl}}$, $M_{\text{lag}}^{\text{bl}}$ | = blade flap and lag moments, Nm |
| $M_u$, $M_w$, etc. | = pitching moment derivatives, 1/(ms), etc. |
| $N_v$, $N_p$, etc. | = yawing moment derivatives, 1/(ms), 1/s, etc. |
| $n$blades | = number of blades |
| $n$elem | = number of blade elements |
| $p$, $q$, $r$ | = angular velocity components about body axes, rad/s |
| $Q_u$, $Q_w$, etc. | = rotor torque derivatives, rev/min/(m), etc. |
| $R$ | = rotor radius, m |
| $r$ | = radial position on rotor disk, m |
| $\boldsymbol{r}_{\text{cg}}$ | = position of center of mass, body axes, m |
| $\boldsymbol{r}_{\text{hinge}}$ | = position of flap, lag and feather hinge, rotor axes, m |
| $\boldsymbol{r}_{\text{hub}}$ | = position of rotor hub, body axes, m |
| $T_{\text{aero}}$ | = aerodynamic thrust, N |
| $T_1$, $T_2$, $T_3$ | = transformation matrices |
| $u$, $v$, $w$ | = translational velocity components along body axes, m/s |
| $\boldsymbol{u}$ | = control vector |
| $u_{\text{hub}}$, $v_{\text{hub}}$, $w_{\text{hub}}$ | = rotor hub velocities in non-rotating reference frame, m/s |
| $v_i(r, \psi)$ | = induced velocity at position $(r, \psi)$, m/s |
| $v_{i_m}$ | = momentum induced velocity, m/s |
| $v_{i_0}$, $v_{1_s}$, $v_{1_c}$ | = components of induced velocity, m/s |
| $v_m$ | = wake mass flow velocity, m/s |
| $v_T$ | = wake velocity, m/s |
| $\boldsymbol{X}$ | = rotor force vector, m |
| $\boldsymbol{X}_{\text{elem}}$, $\boldsymbol{X}_{\text{elem}}^{\text{aero}}$, $\boldsymbol{X}_{\text{elem}}^{\text{inertial}}$ | = blade element contributions to rotor force; total, aerodynamic, inertial, N |
| $X_u$, $X_w$, etc. | = longitudinal body axis acceleration derivatives, 1/s, etc. |
| $\boldsymbol{x}$ | = state vector |
| $\boldsymbol{x}_1$, $\boldsymbol{x}_2$ | = subspace of linearized model state vector |
| $Y_v$, $Y_p$, etc. | = lateral body axis acceleration derivatives, 1/s, m/(rad s), etc. |
| $Z_u$, $Z_w$, etc. | = vertical body axis acceleration derivatives, 1/s, etc. |
| $\eta_c$ | = lateral stick position, % (0% fully left) |
| $\eta_s$ | = longitudinal stick position, % (0% fully forward) |
| $\rho$ | = air density, kg/m$^3$ |
| $[\tau]$ | = time constant matrix, s |
| $\phi$, $\theta$ | = roll and pitch attitude, rad |
| $\chi$ | = wake skew angle, rad |
| $\psi$ | = azimuthal position on rotor disc, rad; yaw attitude, rad |
| $\omega_x^{\text{bl}}$, $\omega_y^{\text{bl}}$, $\omega_z^{\text{bl}}$ | = blade angular velocities, rad/s |

*Subscript*

| | |
|---|---|
| wind | = wind axes |

## Introduction

THE autogyro helped to pave the way for the development of the helicopter, introducing cyclic pitch control and blades attached to the rotor hub by means of a hinge. However, it has found no practical application in commercial or military roles, although the type is very popular for sport and recreational flying. The literature on autogyros (or gyroplanes) is considerable, for example, Refs. 1–11, but this work is now primarily of historical significance. However, a program of study was funded by the U.K. Civil Aviation Authority, following a spate of fatal accidents.[12] This work has sought to establish a rigorous and consistent understanding of the factors influencing autogyro stability, control, and handling qualities. A program of mathematical modeling, simulation, wind-tunnel measurements, and flight testing has examined the characteristics of a single type, the VPM M16 (Fig. 1). Results have been reported elsewhere; Refs. 13–16 separately describe factors influencing longitudinal stability, wind-tunnel testing of a scale-model airframe, and experiments to gather flight-test data for parameter estimation exercises.

Developments in rotorcraft simulation have been driven exclusively by the helicopter problem, and models have undergone

Received 30 November 1998; revision received 15 October 1999; accepted for publication 19 November 1999. 

*Senior Lecturer, Department of Aerospace Engineering. Member AIAA.


**Fig. 1 VPM M16 autogyro.**

continuous development to address deficiencies in their predictive ability that have been highlighted by flight test. They have progressed from simple forms that would be familiar to a fixed-wing flight dynamicist, that is, linearized, small perturbation derivative models, to highly nonlinear models, where each blade is individually represented. The literature contains several key examples of the need for improving models beyond simple forms. Hansen[17] highlighted the importance of blade flap dynamics. Chen and Hindson[18] examined the significance of coupled flap/inflow dynamics in hovering flight, and Tischler[19] showed that modeling coupled roll/lag dynamics was necessary in the context of control system design. All three papers deal with linearized models, two in derivative form and one in transfer function form, and the modeling uses disk, rather than individual blade, representations of the rotors. However, the work does highlight the importance of higher-order dynamics, and in recent years, the associated degrees of freedom have been incorporated in individual blade models that have been developed for piloted simulation.[20–22]

Although an engineering model is a powerful tool for supporting studies into aircraft stability, control, and handling qualities, confidence in the results can only be quantified if the model has a known level of validity. Formal approaches to the general problem of validation do not exist, but model fidelity is generally described in terms of amplitude and frequency, and here this is addressed by comparing trim, linearized small-perturbation derivatives and the response to large-amplitude control inputs. The objective of this paper is to validate a generic rotorcraft mathematical model for simulation of those aspects of autogyro flight that are important in the analysis of stability, control, and handling qualities issues. Specific aims of the work are, first, to demonstrate that a typical generic rotorcraft mathematical model is capable of simulating autogyro flight without special modification and, second, to define the predictive capability across a wide range of operating conditions from steady flight to the transient response to large control inputs. The paper makes a unique contribution to the field because there is no comparable work in the literature that defines a level of validity for a mathematical model simulating rotorcraft flight in autorotation.

## Mathematical Model

### Model Description

The model has been influenced strongly by the literature in the field, taking account of the significance of research by others into individual blade/blade element modeling and dynamic inflow modeling. The key features of the mathematical model used are summarized in Table 1. The model takes the form

$$A\dot{\boldsymbol{x}} = f(\boldsymbol{x}, \boldsymbol{u}) \tag{1}$$

where the state vector $\boldsymbol{x}$ contains the airframe translational and angular velocity, blade flap, lag and feather angles and rates for each blade on each rotor, the induced velocity states for each rotor wake, as well as the angular velocity of both rotors, and the engine torques. Elements of the control vector $\boldsymbol{u}$ are the four controls, which vary with aircraft type, for example, single main and tail rotor configurations will have three main rotor controls and one tail rotor control. Depending on the number of blades on each rotor, there can be up to 100 nonlinear, periodic ordinary differential equations describing the coupled rotor/airframe behavior. Note that the matrix $A$ contains off-diagonal terms not simply associated with airframe products of inertia, but that also include terms associated with the dynamic inflow and blade equations of motion.

**Table 1 Mathematical model description**

| Model item | Characteristics |
|---|---|
| Rotor dynamics (both rotors) | Up to 10 individually-modeled rigid blades<br>Fully coupled flap, lag and feather motion<br>Blade attachment by offset hinges and springs<br>Linear lag damper |
| Rotor loads | Aerodynamic and inertial loads represented by up to 10 elements per blade |
| Blade aerodynamics | Lookup tables for lift and drag as function of angle of attack and Mach number |
| Wake model | Peters' dynamic inflow model<br>Uniform and harmonic components of inflow<br>Rudimentary interaction with tail surfaces ground effect |
| Transmission | Coupled rotorspeed and engine dynamics up to 3 engines<br>Geared or independently controlled rotor torque |
| Airframe | Fuselage, tailplane and fin aerodynamics by lookup tables or polynomial functions |
| Atmosphere | International Standard Atmosphere provision for variation of sea-level temperature and pressure |

The model has been used previously for helicopter validation and simulation studies[23,24] and simulation of autogyros.[13] The induced velocity model, force and moment expressions, and the blade equations of motion are now summarized.

First, the dynamic inflow representation used is taken from Chen,[25] although the original model development is due to Gaonkar and Peters[26] and Peters and HaQuang.[27] The basic form of induced velocity at any azimuth and radial station over the rotor is given by

$$v_i(r, \psi) = v_{i_0} + (r/R)v_{1_s}\sin\psi + (r/R)v_{1_c}\cos\psi \tag{2}$$

The induced velocity $v_i(r, \psi)$ appears explicitly in the aerodynamic model, contributing to the blade element angle of attack. The three states $v_{i_0}$, $v_{1_s}$, and $v_{1_c}$ and are calculated from

$$[\tau]\begin{bmatrix}\dot{v}_{i_0}\\ \dot{v}_{1_s}\\ \dot{v}_{1_c}\end{bmatrix}_{\text{wind}} = -\begin{bmatrix}v_{i_0}\\ v_{1_s}\\ v_{1_c}\end{bmatrix}_{\text{wind}} + [L]\begin{bmatrix}T_{\text{aero}}\\ L_{\text{aero}}\\ M_{\text{aero}}\end{bmatrix}_{\text{wind}} \tag{3}$$

where

$$[\tau] = \begin{bmatrix} \dfrac{4R}{3\pi v_T C_0} & 0 & \dfrac{-R\tan(\chi/2)}{12v_m} \\ 0 & \dfrac{64R}{45\pi v_m(1+\cos\chi)} & 0 \\ \dfrac{5R\tan(\chi/2)}{8v_T} & 0 & \dfrac{64R\cos\chi}{45\pi v_m(1+\cos\chi)} \end{bmatrix} \tag{4}$$

and

$$L = \frac{1}{\rho\pi R^3}\begin{bmatrix} \dfrac{R}{2v_T} & 0 & \dfrac{15\pi\tan(\chi/2)}{64v_m} \\ 0 & \dfrac{-4}{v_m(1+\cos\chi)} & 0 \\ \dfrac{15\pi\tan(\chi/2)}{64v_T} & 0 & \dfrac{-4\cos\chi}{v_m(1+\cos\chi)} \end{bmatrix} \tag{5}$$

Equation (3) is transformed from wind to body axes in this application. The reader is referred to the original literature for detail and history of the development of these equations.

Second, the rotor forces and moments are given by

$$\boldsymbol{X} = T_1^{-1} \sum_{j=1}^{n\text{blades}} \left( T_2^{-1} T_3^{-1} \left\{ \sum_{i=1}^{n\text{elem}} \boldsymbol{X}_{\text{elem}} \right\} \right) \tag{6}$$

$$\boldsymbol{L} = T_1^{-1} \sum_{j=1}^{n\text{blades}} \left( T_2^{-1} \left[ -\boldsymbol{r}_{\text{hinge}} x \left( T_3^{-1} \left\{ \sum_{i=1}^{n\text{elem}} \boldsymbol{X}_{\text{elem}} \right\} \right) \right] \right) + (\boldsymbol{r}_{\text{hub}} - \boldsymbol{r}_{\text{cg}}) x \boldsymbol{X} \tag{7}$$

where

$$\boldsymbol{X}_{\text{elem}} = \boldsymbol{X}_{\text{elem}}^{\text{aero}} + \boldsymbol{X}_{\text{elem}}^{\text{inertial}} \tag{8}$$

The matrices $T_1$, $T_2$, and $T_3$ transform quantities from blade element to rotor and nonrotating airframe axes. Development of these equations is given in Ref. 23.

Finally, the blade equations of motion are based on the derivation given in Ref. 28 and are given by

$$\begin{aligned} I_{\text{flap}} \dot{\omega}_x^{\text{bl}} + \omega_y^{\text{bl}} \omega_z^{\text{bl}} - m_{\text{bl}} y_{\text{cg}}^{\text{bl}} a_z^{\text{hinge}} &= M_{\text{flap}}^{\text{bl}} \\ I_{\text{pitch}} \dot{\omega}_y^{\text{bl}} - \omega_x^{\text{bl}} \omega_z^{\text{bl}} &= M_{\text{pitch}}^{\text{bl}} \\ I_{\text{lag}} \dot{\omega}_z^{\text{bl}} + \omega_x^{\text{bl}} \omega_y^{\text{bl}} + m_{\text{bl}} y_{\text{cg}}^{\text{bl}} a_x^{\text{hinge}} &= M_{\text{lag}}^{\text{bl}} \end{aligned} \tag{9}$$

Again, expressions for the angular velocities $\omega_x^{\text{bl}}$, $\omega_y^{\text{bl}}$, and $\omega_z^{\text{bl}}$ are derived in Ref. 23. Hinge acceleration terms $a_x^{\text{hinge}}$, and $a_z^{\text{hinge}}$ are derived using standard kinematic principles. Note that the applied moment terms $M_{\text{flap}}^{\text{bl}}$ and $M_{\text{lag}}^{\text{bl}}$ include spring restraint terms, to be used if appropriate, and the lag degree of freedom embodies a very rudimentary lag damper term.

The model is, therefore, a very conventional individual blade/blade element representation of a generic two-rotor aircraft. The rotor module is called twice in the simulation code, each rotor being discriminated by data that specify its location and orientation on the airframe and its characteristics in terms of blade mass distribution, hinge offset and restraint, etc. Trim and linearization is performed using the procedure described in Ref. 23. The autogyro configuration, however, requires the linearization process to reduce the model to the form

$$\begin{pmatrix} \dot{\boldsymbol{x}}_1 \\ \dot{\boldsymbol{x}}_2 \end{pmatrix} = \begin{pmatrix} A_{11} & A_{12} \\ A_{21} & A_{22} \end{pmatrix} \begin{pmatrix} \boldsymbol{x}_1 \\ \boldsymbol{x}_2 \end{pmatrix} + \begin{pmatrix} B_1 \\ B_2 \end{pmatrix} \boldsymbol{u} \tag{10}$$

where the conventional six-degree-of-freedom (6-DOF), nine-state model structure is represented by

$$\dot{\boldsymbol{x}}_1 = A_{11} \boldsymbol{x}_1 + B_1 \boldsymbol{u}, \qquad \boldsymbol{x}_1 = [u, v, w, p, q, r, \phi \theta \psi]^T \tag{11}$$

and

$$\dot{\boldsymbol{x}}_2 = A_{21} \boldsymbol{x}_1 + A_{22} \boldsymbol{x}_2 + B_2 \boldsymbol{u}, \qquad \boldsymbol{x}_2 = [\Omega] \tag{12}$$

is the rotorspeed DOF. The minor $A_{12}$ then couples rotor speed into the conventional rigid-body DOF. Note that the treatment of $\Omega$ is in accordance with convention for derivative calculation, that is, it is held constant for calculation of elements in $A_{11}$, $A_{21}$, $B_1$, and $B_2$ and only perturbed for deriving the elements in $A_{22}$ and $A_{12}$.

### Configuration of the Model as an Autogyro

The aircraft used in this study was the VPM M16 gyroplane (Fig. 1). It is of Italian origin, produced in kit form for assembly by the owner. The maximum all-up mass is 450 kg. The aircraft is powered by a four-cylinder two-stroke engine driving a three-bladed fixed-pitch propeller. For helicopter engineers not familiar with gyroplanes, the rotor system is of an interesting configuration, typical of this class of aircraft. The two main rotor blades are bolted to a teeter bar, suspended from a teeter bolt. The blades are untwisted, and no cyclic pitch can be applied. This hub assembly is mounted on a spindle, about 200 mm long, and this spindle pivots about its lower end to tilt the entire rotor fore and aft and laterally to effect pitch and roll control, respectively. The rotor system is linked mechanically by rods to the pilot's control column, and a conventional rudder is operated by a cable assembly from foot pedals.

Two aspects of this aircraft require consideration in relation to the model formulation outlined earlier. First is autorotation because the literature suggests that no consideration has been given to the use of the dynamic inflow model in this mode. Consider $v_T$, $v_m$, and $\chi$. By the neglecting of the contribution of the longitudinal tilt of the rotor disk, which simulation results have shown to be at least an order of magnitude smaller than the rotor angle of attack, then

$$v_T = \sqrt{u_{\text{hub}}^2 + v_{\text{hub}}^2 + \left(v_{i_m} - w_{\text{hub}}\right)^2} \tag{13}$$

$$v_m = \left\{ u_{\text{hub}}^2 + v_{\text{hub}}^2 + \left(v_{i_m} - w_{\text{hub}}\right)\left[2v_{i_m} - w_{\text{hub}}\right] \right\}^{\frac{1}{2}} \tag{14}$$

$$\tan \chi = \frac{\sqrt{u_{\text{hub}}^2 + v_{\text{hub}}^2}}{v_{i_m} - w_{\text{hub}}} \tag{15}$$

In autorotation, $w_{\text{hub}} > v_{i_m}$. Therefore the velocities $v_T$ and $v_m$ will be positive, and for $v_T$ in particular this means that $v_{i_0} > 0$, that is, the flow slows down on passing through the rotor, as it should in autorotation. Note that $\chi < 0$ due to $w_{\text{hub}} > v_{i_m}$ is geometrically consistent with flow in autorotation, but it does mean that those terms in Eq. (5) that couple $v_{i_0}$ and $v_{1_c}$ change sign. The significance in relation to the physical attributes of the real flow is not clear, but the autogyro simulation results are similar to the helicopter case in that there is an upwash component at the front of the rotor disk and downwash at the rear. This is consistent with the intuitive result for circular wings, irrespective of powered or autorotative operation. Inspection of these equations indicates that the model will emulate physical aspects of autorotative behavior, but its efficacy for simulation of autorotation will be defined by the validation results. For example, the lateral stick position is an indirect validation of $v_{1_c}$. It is the case that boundaries defining the various rotor operating states for axial flight have been determined using simple momentum theory, for example, Refs. 28 and 29. Figure 2 shows the location on such a diagram, taken from Ref. 29, of the 14 autogyro configurations simulated here. The arrow indicates progression from low to high airspeed. It is perhaps misleading to represent these autogyro results on such a chart, which is strictly applicable only to axial, as opposed to edgewise, flight. Whatever the applicability, Fig. 2 does serve to represent these autogyro simulations in the context of the very limited literature available on autorotation.

The second aspect of this autogyro configuration requiring consideration is setting the hinge offset term in the model to zero, which can satisfactorily emulate the flight mechanics of teetering rotor systems.[29] In effect, the simulation then models a rotor system with two centrally hinged blades (although the coning mode of a two-bladed articulated rotor is dissimilar to that of a teetering rotor).

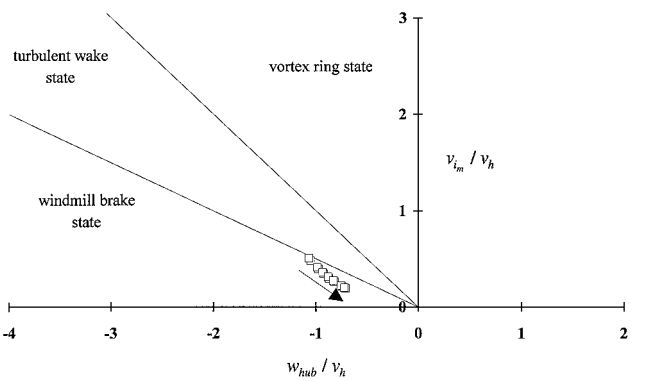


**Fig. 2 Model operating condition in context of typical vertical descent flow states.**

Once again, validation will determine how appropriate this approach is. The simulation is sufficiently generic to allow other aspects of the rotor system and propeller geometry to be accommodated by appropriate data entries or software switches to enable or disable particular features.

Although autogyros have been simulated previously,[30,31] the models and the results obtained were severely limited in their applicability. For example, simple disk representations of the main rotor were used and analytical expressions for linearized stability and control derivatives were formulated. Reference 31 was further limited by using data for a generic aircraft type, that is, a specific aircraft was not modeled. No validation was attempted in either case.

## Results

The simulation model was configured with data appropriate to the flight condition for each test point. Mass and inertia information was available from ground-based measurements. The aircraft mass for each test point was influenced only by fuel state, which could not be measured accurately. Accordingly, simulation results were obtained for the two limiting conditions of full fuel (maximum weight) and zero fuel (minimum weight).

### Equilibrium Flight

Comparison of the model with measurements taken in steady, level flight is shown in Fig. 3. Generally, there is good agreement between model and flight. Simulation of longitudinal stick position compares very favorably with the flight measurement throughout the speed range, indicating that it gives a good prediction of speed stability. Although lateral stick position suffers from a uniform error of about 5% across the speed range, this is less than 0.5 in. of stick displacement. Roll attitude is simulated to within 0.5 deg. The trend in simulated pitch attitude with speed is consistent with flight, although this trend is more accentuated in the simulation giving rise to relatively poor prediction at low speed. Rotor speed trend with speed is simulated accurately by the model, although uniformly in error by about 20–25 rpm. This is considered a good result because rotor speed is not governed to a given value as in helicopter applications.

The deficiencies in validity can be summarized as pitch attitude at low speeds, lateral stick position across the speed range, and to some extent rotor speed. Care is required in assessing the source of discrepancies in rotor speed because it is very sensitive to a variety of parameters such as blade twist (which may manifest itself aeroelastically in flight and is not incorporated in the rigid-blade model), blade incidence angle relative to the hub, and section drag characteristics. The pitch attitude discrepancy could be associated with airframe lift and pitching moment. However, wind-tunnel data for this airframe were obtained for a wide range of angle of attack and sideslip.[14] The contribution of the airframe is weak in relation to the rotor and propeller, especially so at the lower speeds, which tends to suggest that the source of pitch attitude modeling errors lies elsewhere. For example, a simple interpretation of rotor angle of attack

$$\alpha_{\text{rotor}} = \eta_s + \theta + \beta_{1c} \tag{16}$$

tends to suggest that inflow modeling at low speed may be the source of this particular discrepancy. This is because $\eta_s$ is accurately predicted, and $\beta_{1c}$ is typically small (less than 2 deg across the speed range), and so the deficiency in pitch attitude at low speed is most probably due to simulation of rotor angle of attack. Because the deficiency is speed dependent, it is argued that this points to a weakness that is related to physical modeling, rather than inappropriate data such as blade section lift characteristics.

It is also possible to speculate that an inflow modeling deficiency may be responsible for the lateral stick position result, where the model underestimates flight by 5–10% across the speed range. Figure 4 shows the impact of setting the harmonic components of induced velocity ($v_{1_s}$ and $v_{1_c}$) to zero. (Note that $v_{1_s}$ has a negligible impact on lateral stick position, but was set to zero for consistency.) This has little impact above 50 mph, but does improve the result in the lower-half of the speed range. However, a perusal of Chen's survey paper[25] indicates that, at least for powered rotors, there is no evidence that would tend to support the postulate that $v_{1_c}$ might be zero.

### Small-Perturbation Flight: Longitudinal

Figure 5 shows comparisons of key longitudinal stability and control derivatives obtained using the linearization approach outlined earlier and those from flight test.[15] The flight-derived values are presented as 95% confidence bounds, whereas the model results are those for minimum and maximum mass.

Some simulation and flight derivatives show a consistent trend with speed. Simulation values can lie within, or overlap, the uncertainty bounds of the flight results. It is argued that in such cases, model and flight can be said to be in agreement, within the limitations of derivative identifiability and modeling uncertainty. However, certain cases do point to modeling inadequacy that can be classed as moderate to severe. For example, the drag damping term $X_u$, which is of paramount importance in phugoid mode damping, is very poorly predicted by the model. Similarly, heave damping $Z_w$ plays an important role in short-period mode damping, but is substantially overestimated by the simulation model. Of less concern is the mismatch in $M_w$. The model results appear simply shifted relative to the flight values; significantly, the model captures the unusual result for unaugmented rotorcraft, that $M_w < 0$. A physical reasoning for this result is given in Ref. 15. Coupling of rotor speed with

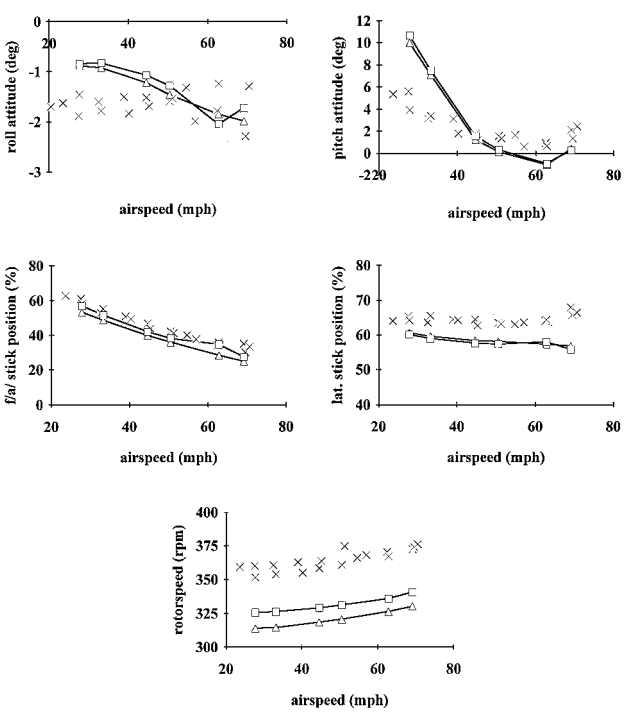


**Fig. 3 Flight and simulation comparisons of key trim parameters: ×, flight data; △, model, minimum weight; and □, model, maximum weight.**

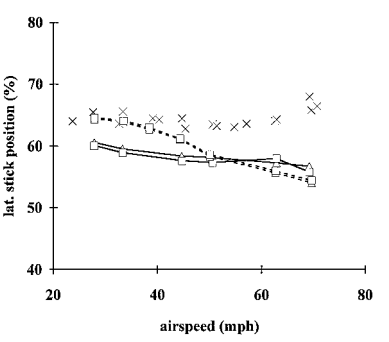


**Fig. 4 Effect of removing harmonic components of induced velocity on lateral stick position: ×, flight data; –△–, model, minimum weight; –□–, model, maximum weight; - -△- -, model, minimum weight no inflow harmonics; and - -□- -, model, maximum weight no inflow harmonics.**

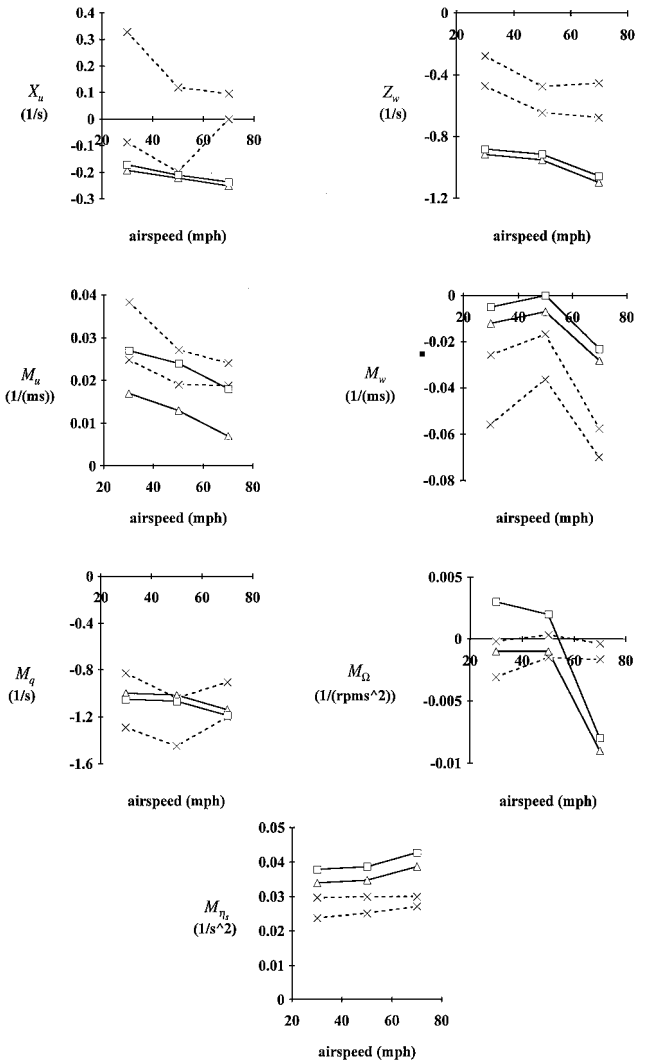


**Fig. 5 Flight and simulation comparisons of key longitudinal derivatives: ×, flight data; △, model, minimum weight; and □, model, maximum weight.**

the pitch DOF manifested in terms of $M_\Omega$ is reasonably represented in the simulation model, except at high speed.

The rotor torque derivatives [Eq. (12)] are unique to rotors in autorotation and are, therefore, of major importance to simulation of autogyros. In addition, given the sensitivity of rotor speed to a multiplicity of factors, good modeling of these terms gives confidence that the physical modeling is accurate. Some of the key derivatives in Eq. (12) are presented in Fig. 6, which shows that the simulation model results exhibit excellent agreement with flight.

The deficiencies in $X_u$ and $Z_w$ and to a lesser extent $M_w$ have a salient impact on the prediction of the modes of motion. Figure 7 shows a comparison between flight and simulation model longitudinal eigenvalues for 30 and 70 mph. Arrows indicate the progression from low to high speed. In general terms, the short-period mode damping is greater in the simulation model because of the overestimate in $Z_w$, which could be attributed to errors in modeling rotorspeed. Blade torsion can have a pronounced effect on thrust, and this may also have a role to play. The slight difference in short-period mode frequency is due to the offset in $M_w$ across the speed range. This could be due to airframe aerodynamics, but previous work[13] has shown this derivative to be sensitive to the vertical location of the center of mass in relation to the propeller thrust line. The phugoid mode damping is of much greater concern. Grossly overestimated by the model, this is directly attributable to the poor prediction of $X_u$. In the simulation, airframe drag characteristics account for about 10% of $X_u$, the bulk coming from the rotor. This

**Table 2 Comparison of flight and simulation lateral/directional derivatives**

| | Flight | | Model | |
|---|---|---|---|---|
| Parameter | Lower bound | Upper bound | Minimum weight | Maximum weight |
| $Y_v$ | −0.133 | −0.044 | −0.194 | −0.179 |
| $L_p$ | −2.727 | −2.377 | −2.714 | −2.822 |
| $L_{\eta_c}$ | 0.060 | 0.067 | 0.078 | 0.085 |
| $L_v$ | 0.028 | 0.041 | 0.172 | 0.142 |
| $N_v$ | 0.055 | 0.063 | 0.064 | 0.060 |
| $N_r$ | −0.996 | −0.812 | −0.104 | −0.091 |

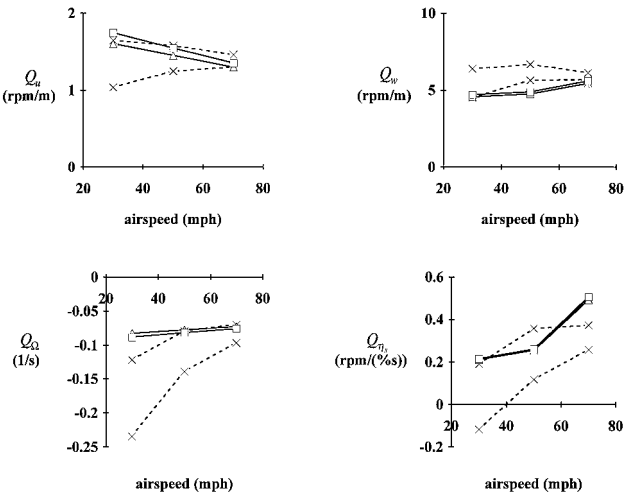


**Fig. 6 Flight and simulation comparisons of key rotor torque derivatives: ×, flight data; △, model, minimum weight; and □, model, maximum weight.**

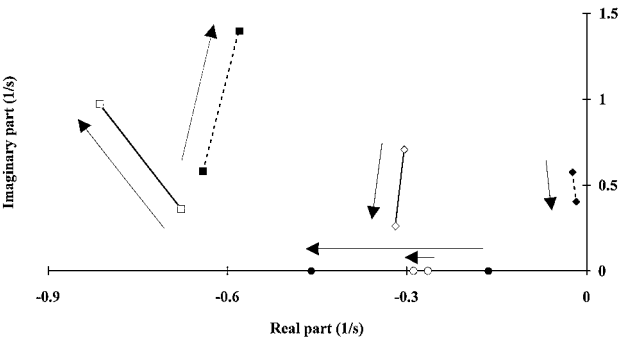


**Fig. 7 Comparison of flight-identified and model eigenvalues: ■, shortperiod; ●, rotorspeed; ◆, phugoid; ◇, phugoid, model; ○, rotorspeed, model; and □, shortperiod, model.**

is consistent with Glauert's elementary theory.[1] Paradoxically, in Ref. 15 it is argued that the flight result is consistent with observed aircraft behavior. It is difficult, therefore, even to speculate as to the source of this discrepancy without further flight tests on aircraft dissimilar to that used for the present study.

### Small-Perturbation Flight Lateral/Directional

Table 2 compares key lateral/directional derivatives from simulation and flight. The flight results are taken from Ref. 16, which focused on 70 mph. The rolling moment derivatives $L_p$ and $L_{\eta_c}$ are dominated by the rotor system, and the simulation displays fair correlation with flight. As in the case of the pitch axis, the model overestimates the control derivative $L_{\eta_c}$. The rotor makes a weak contribution to $L_v$, which is strongly influenced by airframe aerodynamics. The flight results indicate that the aircraft displays lack of dihedral effect, which is because the airframe side area is low relative to the center of mass. The simulation overpredicts the severity of this configuration effect.

The directional derivatives are dominated by airframe aerodynamics, which will also be influenced by propeller slipstream. The simulation model, therefore, depends crucially on the quality of the wind-tunnel test data if good correlation between simulation and flight is to be obtained. It is clear that correlation varies from reasonable to extremely poor. Weathercock effect $N_v$ is reasonably predicted by the model, but correlation in yaw damping $N_r$ is extremely poor.

**Response to Large-Amplitude Inputs**

Figures 8 and 9 show comparisons between flight and the full nonlinear, individual blade/blade element model, for lateral and longitudinal stick inputs at a nominal 70 mph. Note that the simulation displays the high-frequency periodicity associated with modeling individual blades.

The first case considered is shown in Fig. 8. The lateral control stick input measured in flight was used to drive the full nonlinear, individual blade/blade element model. The shape and magnitude of the primary response in roll rate is modeled well by simulation up to about 10 s. This is consistent with the result in Table 2 for $L_p$ and $L_{\eta_c}$, which have a dominant effect on short-term roll response. After the first response peak, the model responds more sharply than the real aircraft. This is not manifestation of a lag due to blade flap dynamics because the interval is too great and in any case such a lag would be apparent during the initial response. The phasing of the off-axis response in pitch rate is surprisingly well modeled up to 10 s as well. Cross coupling remains one of the particular challenges in helicopter modeling, and so why the coupling is so well predicted with the model in the autogyro mode is not clear. Beyond 10 s, the real aircraft is very well damped, whereas the model enters a lightly damped Dutch roll oscillation. This is consistent with comparisons in Table 2, where two derivatives that directly influence the Dutch roll, $L_v$ and $N_r$, compare poorly with flight. The rotor speed response correlation is not as poor as it first appears; there is little short-term response, and this is reflected by the model.

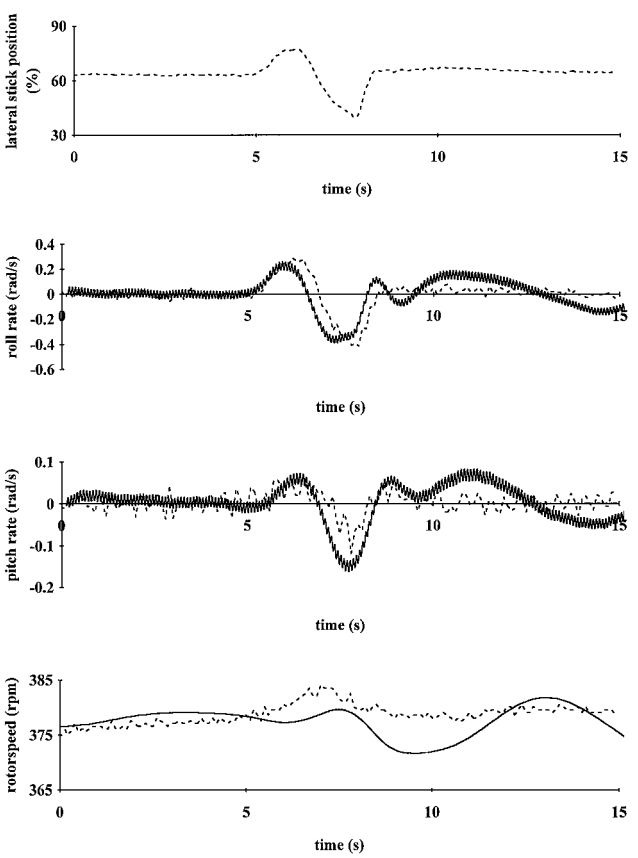


**Fig. 8 Response to lateral stick, comparison of flight and simulation: – – –, flight data, and ——, simulation.**

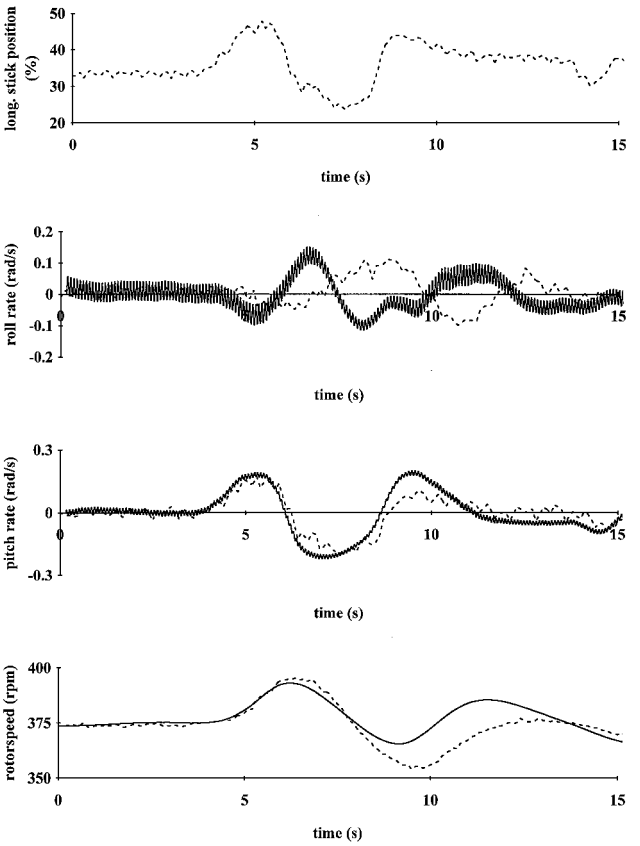


**Fig. 9 Response to longitudinal stick, comparison of flight and simulation: – – –, flight data, and ——, simulation.**

Thereafter, the incorrectly modeled Dutch roll mode dominates the simulation result, whereas the real aircraft, as already noted, is well damped.

Figure 9 shows comparisons of response to a longitudinal stick input. The longer-term rotorspeed response, that is, greater than 10 s, is more heavily damped in the simulation model than in-flight. This is entirely consistent with linearized model validation, which revealed that the real aircraft has little drag damping and, as a result, little phugoid or long-term damping. The opposite is true with the linearized simulation model. The pitch rate response is simulated fairly well, the only anomalous period in time being around 10 s, consistent with the mismatch in rotor speed. However, the off-axis response in roll rate displays behavior familiar to helicopter flight dynamicists, where the amplitude is reasonably predicted in magnitude, but not in phase.

## Discussion

The criteria used to assess whether or not the rotorcraft model can adequately simulate the autogyro are necessarily subjective, relying on engineering judgment because there are no formal criteria for autogyro simulation. However, comparisons with Federal Aviation Administration level D simulator requirements for helicopters[32] can be instructive. They are expressed in terms of trim and time response comparisons, and the model generally satisfies the requirements for control position prediction to be within 5% and attitude to be within 1.5 deg. Primary axis time responses would fall within acceptable envelopes, although the cross coupling would not. The criteria for rotorspeed simulation in autorotation is not pertinent to the autogyro.

Although there are no criteria for derivative comparisons, Tischler[33] is developing criteria for frequency-response validation. It is accepted that the linearized 6-DOF model structure is of limited utility in the context of frequency-responsemethods, being applicable to a much narrower bandwidth. However, the validation envelope defined by the approach taken in this paper is consistent with pilot

control strategy for autogyros, which is essentially low frequency. In addition, the derivative allows a high degree of insight into the causes of specific modeling deficiencies, such as the heavily damped phugoid $X_u$ or under-damped Dutch roll, $L_v$ and $N_r$, which is absent with the aggregate presentation of a frequency response.

Notwithstanding the lack of formal criteria, it is argued that validation discrepancies are typical of that obtained for helicopter models. For example, the poorly predicted directional characteristics are determined largely by airframe aerodynamics that are obtained from wind-tunnel tests. However, discrepancies in the drag and heave damping derivatives $X_u$ and $Z_w$ could be directly attributed to modeling of physical phenomena unique to the autogyro, specifically the induced velocity in autorotation. However, the functionality of the Peters wake dynamic inflow model for the autogyro appears acceptable, and given that no previous autogyro model validation has taken place, a definitive statement cannot be made until the predictive ability of the model for simulating other types reveals whether or not errors in $X_u$ and $Z_w$, in this case, are indicative of a generic problem or are type specific. Note that if the model can simulate autogyro flight, it should in principle be capable of simulating helicopters in this flight regime as well. It is, therefore, important that it is capable of being used without major modification to the underlying physical modeling.

## Conclusions

It would appear that generic rotorcraft simulation models can be used to simulate autogyro flight without any modification to the physical form of the governing equations, although further experimental work with different autogyros is required before a definitive statement can be made. This is because the validation against a specific aircraft type over a range of amplitude and frequency has revealed limitations in fidelity that may be unique to the type in question, rather than the autogyro problem in general. However, in terms of trim and rotor torque derivatives, the model emulates satisfactorily the variability in rotor speed that is a consequence of operation in autorotation. The results are, therefore, of wider relevance and significance, specifically to the simulation of helicopters in autorotation.

## Acknowledgment

This work was conducted for the U.K. Civil Aviation Authority under Research Contract 7D/S/1125. The Project Manager was David Howson.

## References

[1]Glauert, H., "A General Theory of the Autogyro," Aeronautical Research Committee Repts. and Memoranda 1111, London, Nov. 1926.

[2]Lock, C. N. H., "Further Development of Autogyro Theory Parts I and II," Aeronautical Research Committee Repts. and Memoranda 1127, London, March 1927.

[3]Glauert, H., "Lift and Torque of an Autogyro on the Ground," Aeronautical Research Committee Repts. and Memoranda 1131, London, July 1927.

[4]Lock, C. N. H., and Townend, H. C. H., "Wind Tunnel Experiments on a Model Autogyro at Small Angles of Incidence," Aeronautical Research Committee Repts. and Memoranda 1154, London, March 1927.

[5]Glauert, H., and Lock, C. N. H., "A Summary of the Experimental and Theoretical Investigations of the Characteristics of an Autogyro," Aeronautical Research Committee Repts. and Memoranda 1162, London, April 1928.

[6]Wheatley, J. B., "Wing Pressure Distribution and Rotor-Blade Motion of an Autogyro as Determined in Flight," NACA TR 475, 1933.

[7]Wheatley, J. B., "An Aerodynamic Analysis of the Autogyro Rotor with a Comparison Between Calculated and Experimental Results," NACA TR 487, 1934.

[8]Wheatley, J. B., and Hood, M. J., "Full-Scale Wind-Tunnel Tests of a PCA-2 Autogyro Rotor," NACA TR 515, 1935.

[9]Wheatley, J. B., "An Analytical and Experimental Study of the Effect of Periodic Blade Twist on the Thrust, Torque and Flapping Motion of an Autogyro Rotor," NACA TR 591, 1937.

[10]Schad, J. L., "Small Autogyro Performance," *Journal of the American Helicopter Society*, Vol. 10, No. 3, 1965, pp. 39–43.

[11]McKillip, R. M., and Chih, M. H., "Instrumented Blade Experiments Using a Light Autogyro," *Proceedings of the 16th European Rotorcraft Forum*, Glasgow, Scotland, 1990, pp. II.8.4.1–II.8.4.8.

[12]"Airworthiness Review of Air Command Gyroplanes," Air Accidents Investigation Branch Rept., Sept. 1991.

[13]Houston, S. S., "Longitudinal Stability of Gyroplanes," *Aeronautical Journal*, Vol. 100, No. 991, 1996, pp. 1–6.

[14]Coton, F., Smrcek, L., and Patek, Z., "Aerodynamic Characteristics of a Gyroplane Configuration," *Journal of Aircraft*, Vol. 35, No. 2, 1998, pp. 274–279.

[15]Houston, S. S., "Identification of Autogyro Longitudinal Stability and Control Characteristics," *Journal of Guidance, Control, and Dynamics*, Vol. 21, No. 3, 1998, pp. 391–399.

[16]Houston, S. S., "Identification of Gyroplane Lateral/Directional Stability and Control Characteristics from Flight Test," *Proceedings of the Institute of Mechanical Engineers*, Pt. G, Vol. 212, No. G4, 1998, pp. 1–15.

[17]Hansen, R. S., "Toward a Better Understanding of Helicopter Stability Derivatives," *Journal of the American Helicopter Society*, Vol. 29, No. 1, 1984, pp. 15–24.

[18]Chen, R. T. N., and Hindson, W. S., "Influence of Dynamic Inflow on the Helicopter Vertical Response," *Vertica*, Vol. 11, Nos. 1 and 2, 1987, pp. 77–91.

[19]Tischler, M. B., "Digital Control of Highly Augmented Combat Rotorcraft," NASA TM-88346, 1987.

[20]Lehmann, G., Oertel, C.-H., and Gelhaar, B., "A New Approach in Helicopter Real-Time Simulation," *Proceedings of the 15th European Rotorcraft Forum*, Amsterdam, 1989, pp. 62.1–62.17.

[21]DuVal, R. W., "A Real-Time Blade-Element Helicopter Simulation for Handling Qualities Analysis," *Proceedings of the 15th European Rotorcraft Forum*, Amsterdam, 1989, pp. 59.1–59.18.

[22]Meerwijk, L., and Brouwer, W., "Real-Time Helicopter Simulation Using the Blade-Element Method," *Proceedings of the 17th European Rotorcraft Forum*, DGLR, Berlin, 1989, pp. 599–616.

[23]Houston, S. S., "Validation of a Non-Linear Individual Blade Rotorcraft Flight Dynamics Model Using a Perturbation Method," *Aeronautical Journal*, Vol. 98, No. 977, 1994, pp. 260–266.

[24]Houston, S. S., "Validation of a Blade-Element Helicopter Model for Large-Amplitude Manoeuvres," *Aeronautical Journal*, Vol. 101, No. 1001, 1997, pp. 1–7.

[25]Chen, R. T. N., "A Survey of Non-Uniform Inflow Models for Rotorcraft Flight Dynamics and Control Applications," *Vertica*, Vol. 14, No. 2, 1990, pp. 147–184.

[26]Gaonkar, G. H., and Peters, D. A., "A Review of Dynamic Inflow Modeling for Rotorcraft Flight Dynamics," *Vertica*, Vol. 12, No. 3, 1988, pp. 213–242.

[27]Peters, D. A., and HaQuang, N., "Dynamic Inflow for Practical Applications," *Journal of the American Helicopter Society*, Vol. 33, No. 4, 1988, pp. 64–68.

[28]Bramwell, A. R. S., *Helicopter Dynamics*, Arnold, London, 1976, pp. 1–13.

[29]Johnson, W., *Helicopter Theory*, Princeton Univ. Press, Princeton, NJ, 1980, pp. 237, 238.

[30]Brotherhood, P., "Stability and Control of the Wallis W117 Autogyro," Royal Aircraft Establishment, TM Aero. 1461, Dec. 1972.

[31]Arnold, U. T. P., "Untersuchungen zur Flugmechanik eines Tragschraubers," Technische Univ. Braunschweig Diplomarbeit 88-5D, Brunswick, Germany, March 1988.

[32]"Helicopter Simulator Qualification," U.S. Dept. of Transportation, Federal Aviation Administration Advisory Circular AC 120-63, Washington, Nov. 1994.

[33]Tischler, M. B., "Digital Control of Highly Augmented Combat Rotorcraft," NASA TM-88346, May 1987.